Angewandte Chemie
Eine Zeitschrift der Gesellschaft Deutscher Chemiker

Supporting Information

Dynamic Release of Bending Stress in Short dsDNA by Formation of a Kink and Forks**

*Cheolhee Kim, O-chul Lee, Jae-Yeol Kim, Wokyung Sung, and Nam Ki Lee**

anie_201502055_sm_miscellaneous_information.pdf

Supplementary Text

The effect of mismatch on dsDNA flexibility

We examined the effect of mismatch in the middle of dsDNA on its flexibility. Fields et al. reported that kink formation correlates highly with thermodynamic energy destabilization by a single-bp mismatch.[1] We varied the number of mismatches (1-3 bp) at the center of the dsDNA portion for all D-samples to increase the range of destabilization energy by mismatches (Supplementary Figure 3). As the number of mismatches increased, the conformer II population increased, but the conformer I population decreased. Interestingly, single (m1) and double (m2) mismatches showed heterogeneous FRET distributions when the ssDNA string length was greater than 8 nt (Supplementary Figure 3 a and b). For R34S30, a single mismatch presented two conformers, but a double mismatch only yielded conformer II. However, all D-samples presented only conformer II with triple bp mismatch (Figure 2 a). The results imply that the dsDNA portion retains considerable rigidity even in the presence of single and double mismatches; thus, it resists the bending force applied by the ssDNA string under our measurement conditions. The population ratio of conformer II is nearly proportional to the estimated destabilization energy due to mismatches (Supplementary Figure 3 c).[2] The destabilization energy was estimated from the free energy penalty by mismatches, i.e., the difference between the free energies of the complementary DNA sequence and mismatched DNA sequence.[1-2] With triple bp mismatch, all D-samples lose their ability to convert into conformer I and, thus, conformer II becomes a permanently stable conformation.

Conformer II includes a kink with local melting (S1 endonuclease test)

Two types of DNA kinks have been suggested based on conservation of base pairing. One type of kink preserves base pairing,[3] which was suggested by Crick and Klug.[4] The second type of kink includes single-stranded DNA due to melting through strong bending.[5] Whether base pairing is conserved or not

when dsDNA develops a kink remains controversial. Recent studies using DNA mini-circles and 'molecular vise' DNA nanostructures suggested the presence of the second type of kink with local melting.[1, 3b]

Because a triple bp mismatch only yields conformer II without conformer I, it is reasonable to assume that all of the D-samples with triple bp mismatch in Figure 2 a include a kink structure due to the bending force exerted by the ssDNA string. We then compared the *E* values of the conformer II with and without mismatches (Supplementary Figure 6 a-c). We noted that for R42S30, R44S30, R46S30, and R60S30, the high FRET efficiency (conformer II) between the mismatched (black line) and completely matched D-samples (red line) exhibited large differences (Supplementary Figure 6 a). By contrast, R34S30, R38S30, and R40S30 presented nearly identical *E* values, regardless of whether mismatches were present (Supplementary Figure 6 b). These results indicate that the high FRET states of the intact D-samples exhibited as much high flexibility as the triple bp mismatched D-samples for R34S30, R38S30, and R40S30, but not for R42S30, R44S30, R46S30, and R60S30 (Supplementary Figure 6 c). These results suggest that up through R42S30, conformer II maintains a bending state. However, when the ssDNA string is shorter than 10 nt, the dsDNA portion seems to include a kink conformation.

Next, we analyzed ***E*** values of D-samples as a function of the Mg^{2+} concentration (Supplementary Figure 6 d). As previously mentioned, Mg^{2+} enhances the flexibility of dsDNA and has an effect of inducing the kink form.[3b, 6] Interestingly, the ***E*** values of R42S30, R44S30, and R46S30 did not exhibit a notable dependence on the Mg^{2+} concentration (Supplementary Figure 6 d and e). However, R38S30 and R40S30 exhibited a significant increase in the FRET efficiency. The sudden increase in the ***E*** values of R38S30 and R40S30 due to Mg^{2+} can be explained by kink state formation, which may accompany a drastic change in the end-to-end distance of the dsDNA portion compared with simple bending. For R42S30, R44S30, and R46S30, the tension applied by the ssDNA string is insufficient to induce a kink even at a high Mg^{2+} concentration. This explanation is consistent with our analysis of mismatched D-samples in

Supplementary Figure 6 c, which also supports the notion that a DNA kink occurs when the length of ssDNA string is shorter than 10 nt.

To support our suggestion that conformer II is in a kink state with local melting, we used S1 endonuclease, which specifically cleaves ssDNA, to test whether the conformer II in this study includes a melting region at the central dsDNA portion (Supplementary Figure 7 and Supplementary Methods). If conformer II includes a local melt at the central dsDNA portion, S1 endonuclease will cleave the central dsDNA portion; thus, ssDNA bands shorter than 30 nt will be elucidated. After an S1 endonuclease treatment, the cleavage products were detected through denaturing polyacrylamide gel electrophoresis (PAGE) (Supplementary Figure 7). D-samples with triple bp mismatch, which include a melting region at the central dsDNA portion, were used as positive controls. Indeed, all samples with mismatches presented a band lower than 30 nt, including R60S30-m3 and linear dsDNA (L40S30-m3). In contrast, linear dsDNA (L40S30) without mismatches served as a negative control and was not cleaved by S1 endonuclease. D-samples without mismatches presented a band that corresponded to a 15 nt oligo when the ssDNA string was shorter than 14 nt. In contrast, R60S30 did not exhibit a band that corresponded to a 15 nt oligo, which indicates that R60S30 has no melting region. It is to be noted that R44S30 was cleaved by S1 endonuclease although single-molecule measurements using R44S30 supports no kink formation. This discrepancy may have occurred by Zn^{2+}, which facilitates a kink;[1] 1 mM Zn^{2+} was added to the cleavage reaction because S1 endonuclease requires Zn^{2+} for enzymatic activity. Overall, the S1 endonuclease measurements support that conformer II is in a kink state with dsDNA melting, which is consistent with previous studies that reported kink formation when dsDNA is highly bent.[1, 7]

Estimation of the radius of dsDNA curvature for kink formation

Using simple models, we estimated the radius of dsDNA curvature for kink formation. Our result suggests that R40S30 is in a boundary structure that includes a DNA kink. Using the simple approximation that a

single ssDNA nt is 0.7 nm long and a single dsDNA bp is 0.34 nm long,[8] the curvature radius of R40S30 was calculated to be 3.5 nm. Next, we again calculated the curvature of the R40S30 radius using the assumption that the bending force of the dsDNA portion is in equilibrium with the stretching force of the ssDNA portion in the D-samples (Supplementary Methods and Supplementary Figure 9 a).[1] A WLC model was used to calculate the dsDNA bending force, and the ssDNA string stretching force was calculated using three types of models: a WLC, a freely jointed chain (FJC),[9] and mean field WLC.[10] All models exhibited a similar trend in compressive bending force, which depended on the ssDNA ring size (Supplementary Figure 9 b). As a result, the R40S30 curvature radius was estimated at ~ 3 nm. The 3 - 3.5 nm curvature corresponds to approximately 56 – 65 bp dsDNA for cyclization. This result is consistent with another study that used closed minicircles composed of dsDNA and concluded that minicircle DNA molecules that are smaller than 65 bp (the DNA curvature radius < 3.5 nm) can include a kink.[3b] Philips and coworkers also predicted that the inner loop radius in bacteriophage DNA packing is small as approximately 3 nm.[11] Because kink formation accompanies melting of a few dsDNA bp, the critical curvature of kink formation should depend on the ionic strength of the buffer and temperature.

Supplementary method

DNA sequences (Random sequences were used for sample preparation)

1. ssDNA ring sequences

Name	Sequence
34 nt	**/5Phos/TACCT/iAmMC6T/AGAACAGATCGCACCTATTGATATGGAT**
38 nt	**/5Phos/TATACCT/iAmMC6T/AGAACAGATCGCACCTATTGATATGGATAT**
40 nt	**/5Phos/CTATACCT/iAmMC6T/AGAACAGATCGCACCTATTGATATGGATATT**
42 nt	**/5Phos/TCTATACCT/iAmMC6T/AGAACAGATCGCACCTATTGATATGGATATTT**
44 nt	**/5Phos/TTCTATACCT/iAmMC6T/AGAACAGATCGCACCTATTGATATGGATATTTC**
46 nt	**/5Phos/CTTCTATACCT/iAmMC6T/AGAACAGATCGCACCTATTGATATGGATATTTCA**
60 nt	**/5Phos/ACTATTGCTTCTATACCT/iAmMC6T/AGAACAGATCGCACCTATTGATATGGATATTTCACCTACCA**

- Atto 550 was labeled at /iAmMC6T/.
- Red color denotes dsDNA part for D-samples.

2. The 30 nt complementary ssDNA sequences

Name	Sequence
S30	**CCA/iAmMC6T/ATCAATAGGTGCGATCTGTTCTAAGG**
S30-m1	**CCA/iAmMC6T/ATCAATAGGTACGATCTGTTCTAAGG**
S30-m2	**CCA/iAmMC6T/ATCAATAGGTATGATCTGTTCTAAGG**
S30-m3	**CCA/iAmMC6T/ATCAATAGGTATAATCTGTTCTAAGG**

- Atto 647N was labeled at /iAmMC6T/.
- The blue color denotes mismatched sequences.

D-sample preparation

We prepared seven different lengths of ssDNA rings (R34, R38, R40, R42, R44, R46, and R60) and four linear ssDNA molecules (S30, S30-m1, S30-m2, and S30-m3). All oligomers were purchased from

Integrated DNA Technologies. The 5' end of the ssDNA was modified by phosphorylation for ssDNA cyclization to form the ssDNA ring. Amine-modified dT was added for dye labeling to both the ssDNA ring and complementary ssDNA. The labeling position was 4 base-pairs from the dsDNA and ssDNA junction. We used Atto550 (SIGMA-ALDRICH) to label the ssDNAs, which were cyclized to form a ring structure. The 30 bp complementary ssDNA was labeled with Atto 647N (SIGMA-ALDRICH). The labeled ssDNAs were purified using a denaturing PAGE gel. Linear dsDNA samples were prepared by annealing ssDNA (L34, L38, L40, L44, L60) with 30 bp complementary ssDNA (S30) as a control. Atto 550-labeled ssDNA molecules were used to form rings. Atto 550-labeled ssDNA molecules were annealed with ligase oligos that consists of a 16 nt complementary sequence at both ends of the Atto550-labeled ssDNA (8 nt for each end).[12] Next, T4 DNA ligase (TAKARA) was added to ligate both ends of the dye-labeled ssDNA. Linear ssDNA without ligation, dimer, and tetramer, and ssDNA complex with ligase, etc, can be generated as a byproduct; these were removed through separation on a denaturing PAGE gel. Next, we tested whether the purified oligos were intact ssDNA rings by adding Exonuclease I (New England Biolabs), which removes all linear ssDNA molecules, but not ssDNA rings. Finally, an Atto 550-labeled ssDNA ring was annealed with S30 to form D-samples (Supplementary Figure 1). All samples were stocked at 4°C in a buffer (20 mM Tris-HCl pH 8.0, 400 mM NaCl). The D-samples with mismatches were generated by annealing the ssDNA rings with S30-m1, S30-m2, or S30-m3.

Single-molecule alternating laser excitation (ALEX) setup

The single-molecule alternating laser excitation method has been previously described.[13] In ALEX, two lasers are used, one for donor excitation (532 nm laser; TECGL-20, World Star Tech) and one for acceptor excitation (633 nm laser; 25-LHP-925, Melles-Griot), which were alternated using acousto-optic

modulators (23080-1, Neos technologies) at a 100 μs period (Supplementary Figure 2 a). Two laser lights were coupled using a dichroic mirror (z532bcm, Chroma) and then focused at 20 μm from the coverslip surface on an objective (water-immersion, 60 X, NA 1.2, UPLAPO) after reflection using a dichroic mirror (Z532/633RPC, Chroma) in an inverted microscope (IX 51, OLYMPUS). The donor and acceptor excitation laser intensities were 80 μW and 30 μW, respectively, before the objective lens in the alternating mode. The fluorescence emissions of freely-diffusing DNA samples were collected through the objective, passed through a 100 μm pinhole, separated into two pathways by a beam splitter (625DCLP, Chroma), and then refocused onto avalanche photodiodes (APDs) (SPCM AQR-13, EG&G Perkin Elmer). Two APDs were used to detect the Atto550 and Atto647N emissions, respectively. HQ580/60m and HQ660LP were used to filter the Atto550 and Atto647N emissions before the APDs, respectively.

Data acquisition and calculating the FRET value (*E*) and stoichiometry parameter (*S*)

The typical excitation volume in our measurement was ~1 fl, and samples were diluted to 50 pM using the single-molecule buffer (20 mM Tris-HCl pH 8.0, 100 mM NaCl, 5% Glycerol(v/v), 1 mM MEA, 100 ug/ml BSA, and 2 mM $MgCl_2$) to ensure detection of a single-molecule. The in-and-out event of a molecule through the excitation volume (~ 1 fl) yielded a burst of fluorescent signal in the time traces (Supplementary Figure 2 b). The fluorescent bursts that corresponded to individual molecules were selected when the photon-count was greater than 25 at a 1 ms time binning (Supplementary Figure 2 b). Each single burst includes three types of fluorescent intensities in the ALEX measurement: I_D^A denotes acceptor dye fluorescent emissions due to a donor-excitation laser, which is a FRET signal; I_D^D donor dye fluorescent emissions due to a donor-excitation laser; and I_A^A acceptor dye fluorescent emissions

due to an acceptor-excitation laser (Supplementary Figure 2 b). These three types of photon-counts were used to calculate ***E*** and ***S*** values of each molecule. The detailed method for calculating ***E*** and ***S*** has been extensively described in previous works.[14] ***E*** and ***S*** are calculated as the ratios of three types of photon-counting using the following equation.

$$E = \frac{I_D^A}{I_D^D + I_D^A}, \qquad S = \frac{I_D^D + I_D^A}{I_D^D + I_D^A + I_A^A}.$$

E reports the distance (***R***) between donor and acceptor dyes with the relationship $R = R_0(\frac{1}{E} - 1)^{\frac{1}{6}}$, where R_0 denotes the Förster radius.[14b] The R_0 of the Atto550-Atto647N pair has been reported as approximately 6.5 nm (https://www.atto-tec.com). ***S*** describes the labeling status of the molecules detected. For donor-only species, I_A^A=0; thus, the ***S*** value for donor-only species equals ~ 1. In the same manner, acceptor-only species yields $I_D^D + I_D^A$=0; thus, the ***S*** value for the acceptor-only species equals ~ 0. D-samples with both donor and acceptor dyes yield S = 0.5. We selected D-samples from the two-dimensional ***E-S*** graph (Supplementary Figure 2 c) that were within the range 0.25 < S < 0.75 (yellow box in Supplementary Figure 2 c). Next, the selected bursts were used to construct a one-dimensional ***E*** histogram, which is presented in the upper area of the ***E-S*** graph. The ratio of the detection channel efficiency (γ) is approximately 1, and the leakage (detection of donor emission by the acceptor detection channel) and the direct excitation of the acceptor due to the donor excitation laser were corrected as previously described.[13] All data were collected at room temperature (22 ± 0.3℃) unless indicates otherwise. All data were acquired and analyses performed using a home-made program constructed using LABVIEW software (National Instrument).

Real-time measurement of D-sample conformational dynamics

ALEX measurement is optimal for measuring the heterogeneity of biomolecules in a buffer solution, due to the short observation time (approximately 1 ms).[13-14] However, the conformational dynamics of biomolecules in a millisecond scale can be observed by increasing the photon-counting rate.[15] To observe the real-time conformational dynamics of D-sample, we applied a high power laser (250 kW/cm^2) and photoprotection buffer[15] (20 mM Tris-HCl pH 8.0, 100 mM NaCl, 2 mM $MgCl_2$, 10% glycerol, 10 mM cysteamine, 1 mM trolox, and 0.01% BSA) to our ALEX measurement. A typical photon-counting rate of ALEX is 30 photons/ms with 10 kW/cm^2 laser excitation and single-molecule buffer (Supplementary Figure 2 b). With a high power laser excitation and photoprotection buffer, however, the photon-counting rate of bursts increased to approximately 100 photons/ms, which is sufficient for 0.3 ms temporal resolution on the FRET time-trace (Figure 3 a). In addition, we increased the concentration of glycerol from 5% to 10%, which increased the viscosity of buffer. The increased viscosity reduced the diffusion speed of D-samples in solution and thus increased the burst duration time. When ALEX was performed with a typical power and single-molecule buffer, single-molecule bursts longer than 8 ms were rarely observed. However, by applying a high power laser with photoprotection buffer, we could obtain approximately 180 bursts, longer than 8 ms with 100 photons/ms counting rate, in a 10 min measurement.

Cleavage assay using S1 endonuclease

Purify doubly labeled D-samples was not necessary for the single-molecule study because the ALEX method can distinguish D-samples from a non-hybridized ssDNA ring and S30. However, for the S1 endonuclease assay, we prepared D-samples by annealing the ssDNA ring and S30 at a 3:1 ratio to ensure that all S30 oligos were hybridized with the ssDNA ring. We mixed 25 nM D-samples with 89 units of S1

endonuclease in a reaction buffer (20 mM Tris-HCl pH 8.0, 100 mM NaCl, 5 % Glycerol, 1 mM $MgCl_2$, and 1 mM $ZnCl_2$ for enzyme activity), which were incubated for 1 hour at room temperature. The cleave products were applied to a denaturing (7 M urea) 20 % polyacrylamide gel electrophoresis (PAGE) gel. Next, we obtained fluorescent gel images using a Typhoon Trio imager (GE healthcare).

Estimation of bending curvature for kink generation

We calculated the curvatures of the radius of the D-samples assuming that the bending force of the dsDNA portion is in equilibrium with the ssDNA stretching force in D-samples. The bending energy is well-known ($E_b = \frac{k_B T}{2}\frac{L_{Pds}}{R^2}L$) based on the Worm Like Chain (WLC) model, where *R* is the radius of the dsDNA circular arc, *L* is the dsDNA contour length, L_{Pds} is the dsDNA persistence length (~50 nm), T is the temperature (295 K in this calculation), and k_B is the Boltzmann constant. Assuming that the bending force of the dsDNA portion and the ssDNA string stretching force are in equilibrium (Supplementary Figure 9 a), the boundary condition can be described as follows.

$$\frac{dE_b}{dz} = \frac{d\theta}{dz}\frac{d}{d\theta}E_b = f_b = f_S$$

, where f_s denote the ssDNA string stretching force. The ssDNA string stretching force can be formulated using the WLC model as described below.[16]

$$\mathrm{f}_s = \frac{\mathrm{k_B T}}{\mathrm{L_{pss}}}\left[\frac{1}{4(1-z/l)^2} - \frac{1}{4} + \frac{z}{l}\right]$$

, where z denotes the end-to-end distance of the ssDNA string, $\mathrm{L_{pss}}$ is the ssDNA persistence length (3 nm), and l is the ssDNA string size. These equations were analytically solved using the conformational

relationship, the curvature of radius $R = \frac{L}{2\pi-\theta}$ and $z = 2R\sin\frac{\theta}{2}$ (Supplementary Figure 9 a). Supplementary Figure 9 b presents the bending force of the dsDNA portion as a function of the ssDNA ring size. To calculate the ssDNA string stretching force, we tested the freely joint chain (FJC) model, the mean-field WLC model and the WLC model. Using these estimates, R40S30, which includes a kink, presented an approximately 3 nm radius curvature.

SI References

[1] A. P. Fields, E. A. Meyer, A. E. Cohen, *Nucleic Acids Res.* **2013**, *41*, 9881-9890.

[2] J. SantaLucia, Jr., D. Hicks, *Annu. Rev. Biophys. Biomol. Struct.* **2004**, *33*, 415-440.

[3] a) F. Lankas, R. Lavery, J. H. Maddocks, *Structure* **2006**, *14*, 1527-1534; b) Q. Du, A. Kotlyar, A. Vologodskii, *Nucleic Acids Res.* **2008**, *36*, 1120-1128.

[4] F. H. Crick, A. Klug, *Nature* **1975**, *255*, 530-533.

[5] a) J. Yan, J. F. Marko, *Phys. Rev. Lett.* **2004**, *93*, 108108; b) Q. Du, C. Smith, N. Shiffeldrim, M. Vologodskaia, A. Vologodskii, *Proc. Natl. Acad. Sci. USA.* **2005**, *102*, 5397-5402; c) P. A. Wiggins, R. Phillips, P. C. Nelson, *Phys. Rev. E* **2005**, *71*, 021909.

[6] a) R. Owczarzy, B. G. Moreira, Y. You, M. A. Behlke, J. A. Walder, *Biochemistry* **2008**, *47*, 5336-5353; b) L. D. Williams, *Annu. Rev. Biophys. Biomol. Struct.* **2000**, *29*, 497-521; c) H. Qu, Y. Wang, C. Y. Tseng, G. Zocchi, *Phys. Rev. X* **2011**, *1*, 021008; d) M. O. Fenley, G. S. Manning, N. L. Marky, W. K. Olson, *Biophys. Chem.* **1998**, *74*, 135-152.

[7] A. Vologodskii, M. D. Frank-Kamenetskii, *Nucleic Acids Res.* **2013**, *41*, 6785-6792.

[8] S. B. Smith, Y. J. Cui, C. Bustamante, *Science* **1996**, *271*, 795-799.

[9] a) P. J. Flory, *Principles of Polymer Chemistry*, Cornell University Press, Ithaca, USA, **1971**; b) O. C. Lee, W. Sung, *Phys. Rev. E* **2012**, *85*, 021902.

[10] S. Jun, J. Bechhoefer, B. Y. Ha, *Europhys. Lett.* **2003**, *64*, 420-426.

[11] P. Grayson, A. Evilevitch, M. M. Inamdar, P. K. Purohit, W. M. Gelbart, C. M. Knobler, R. Phillips, *Virology* **2006**, *348*, 430-436.

[12] a) H. Shroff, B. M. Reinhard, M. Siu, H. Agarwal, A. Spakowitz, J. Liphardt, *Nano Lett.* **2005**, *5*, 1509-1514; b) H. Shroff, D. Sivak, J. J. Siegel, A. L. McEvoy, M. Siu, A. Spakowitz, P. L. Geissler, J. Liphardt, *Biophys. J.* **2008**, *94*, 2179-2186.

[13] C. Kim, J. Y. Kim, S. H. Kim, B. I. Lee, N. K. Lee, *Chem. Commun.* **2012**, *48*, 1138-1140.

[14] a) A. N. Kapanidis, N. K. Lee, T. A. Laurence, S. Doose, E. Margeat, S. Weiss, *Proc. Natl. Acad. Sci. USA.* **2004**, *101*, 8936-8941; b) N. K. Lee, A. N. Kapanidis, Y. Wang, X. Michalet, J. Mukhopadhyay, R. H. Ebright, S. Weiss, *Biophys. J.* **2005**, *88*, 2939-2953.

[15] L. A. Campos, J. W. Liu, X. Wang, R. Ramanathan, D. S. English, V. Munoz, *Nat. Methods* **2011**, *8*, 143-146.

[16] J. F. Marko, E. D. Siggia, *Macromolecules* **1995**, *28*, 8759-8770.

Supplementary Figures

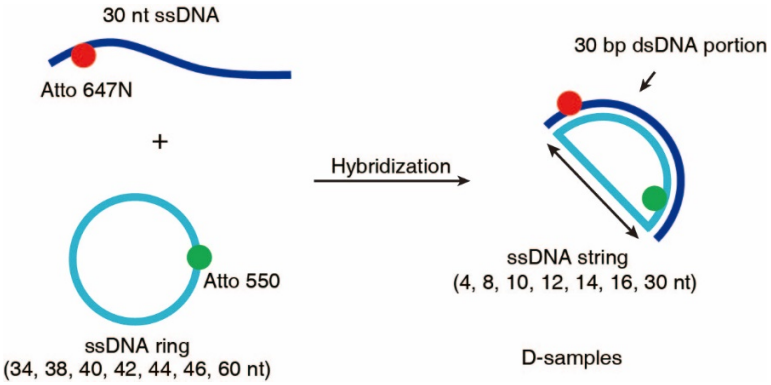

Supplementary Figure 1. Schematic description of doubly labeled D-shaped DNA nanostructures (D-samples). Bending in the dsDNA portion occurs by the stretching force of ssDNA string.

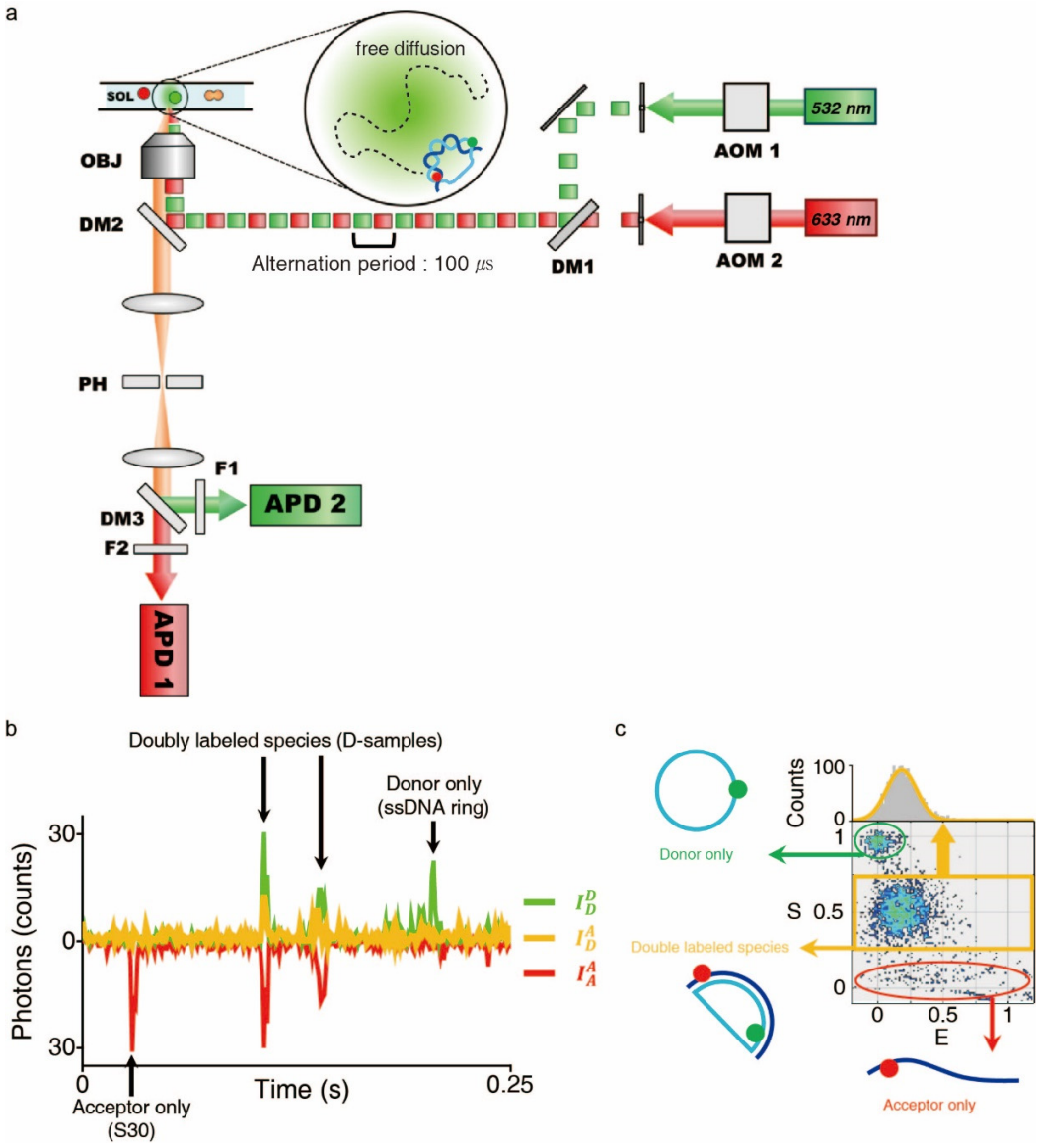

Supplementary Figure 2. (a) Schematic description of alternating-laser excitation single-molecule microscopy. OBJ denotes objective lens, DM denotes dichroic mirror, F denotes filter, APD denotes avalanche photodiode, PH denotes pinhole, and AOM denotes acoustic optical modulator. The alternating period for the two lasers was 100 μs. (b) Time traces obtained using ALEX measurements. A fluorescent burst indicates an event of a single molecule passing through the excitation volume. I_D^D is the fluorescent emission of donor dyes excited by the donor-excitation laser (green line); I_D^A is the fluorescent emission

of acceptor dyes excited by the donor-excitation laser (orange line), which is a FRET signal; and I_A^A is the fluorescent emission of acceptor dyes excited by the acceptor-excitation laser (red line). (c) Two dimensional ***E-S*** graph obtained using ALEX measurements. Donor-only, green ellipse; acceptor-only, red ellipse; doubly labeled species; yellow box. Doubly labeled species were graphically selected from the ***E-S*** graph and were used to construct a one-dimensional FRET histogram.

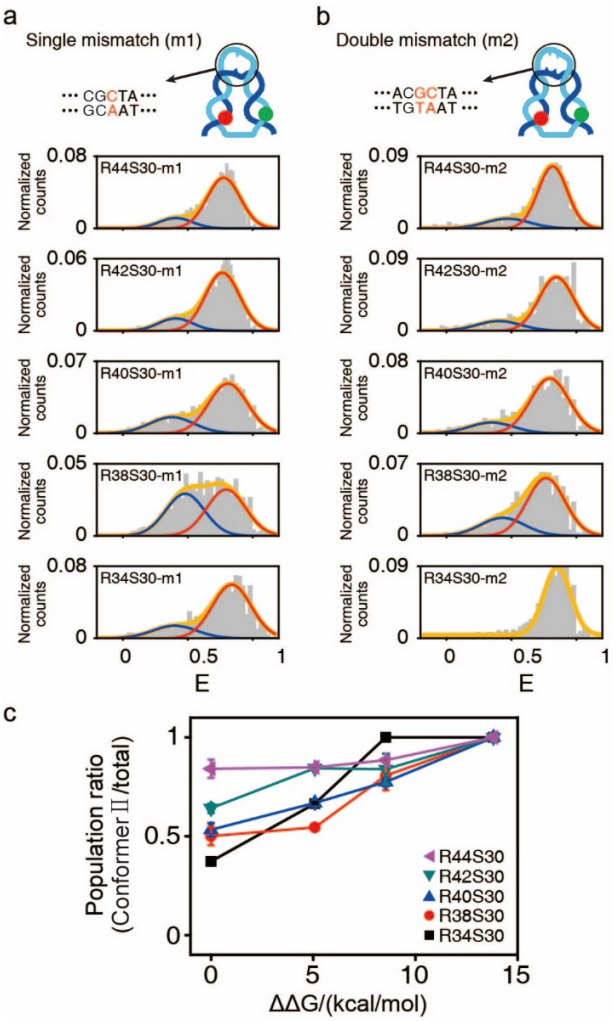

Supplementary Figure 3. The effect of the mismatch number on the subpopulation of D-samples. FRET efficiency histograms for D-samples with (a) a single mismatch or (b) a double mismatch. (c) The sub-population ratio for conformer II (high FRET) as a function of the destabilization energy due to mismatches. The destabilization energies (ΔΔG) for single, double, and triple mismatches were 21, 36 and 58 kJ/mol, respectively, which were calculated based on SI ref. 2.

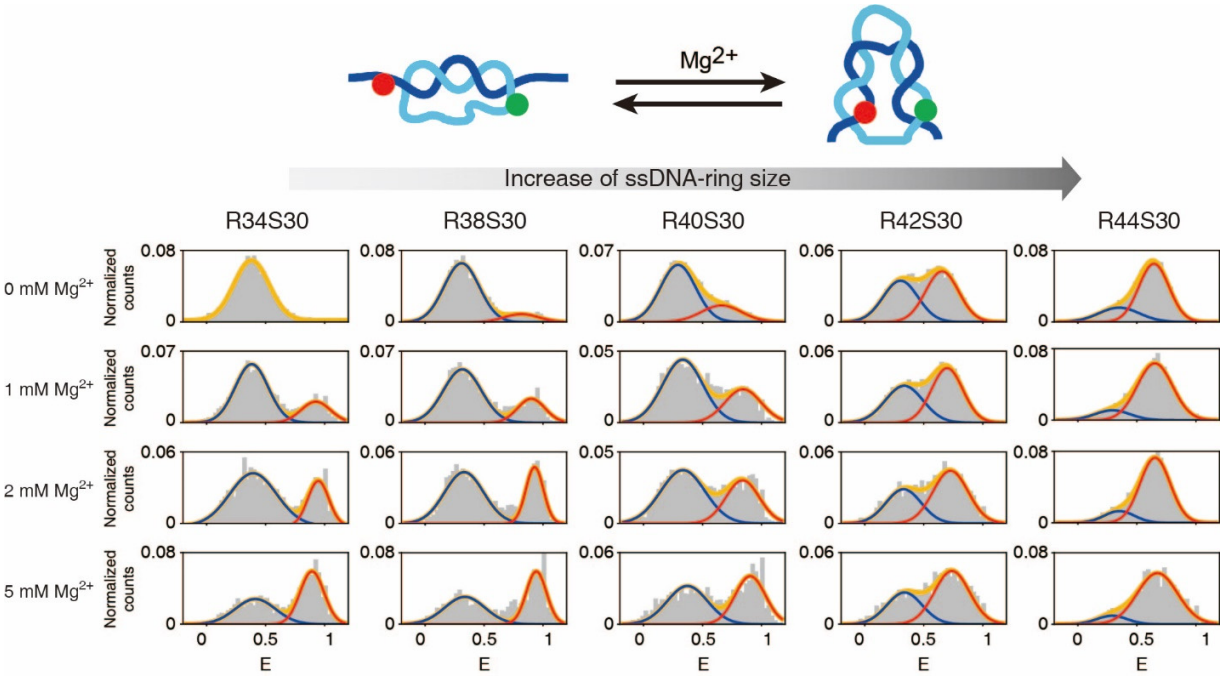

Supplementary Figure 4. FRET efficiency histograms for R34S30, R38S30, R40S30, R42S30, and R44S30 as a function of the Mg^{2+} concentration. The high FRET species sub-population (conformer II) increased as the Mg^{2+} concentration increased.

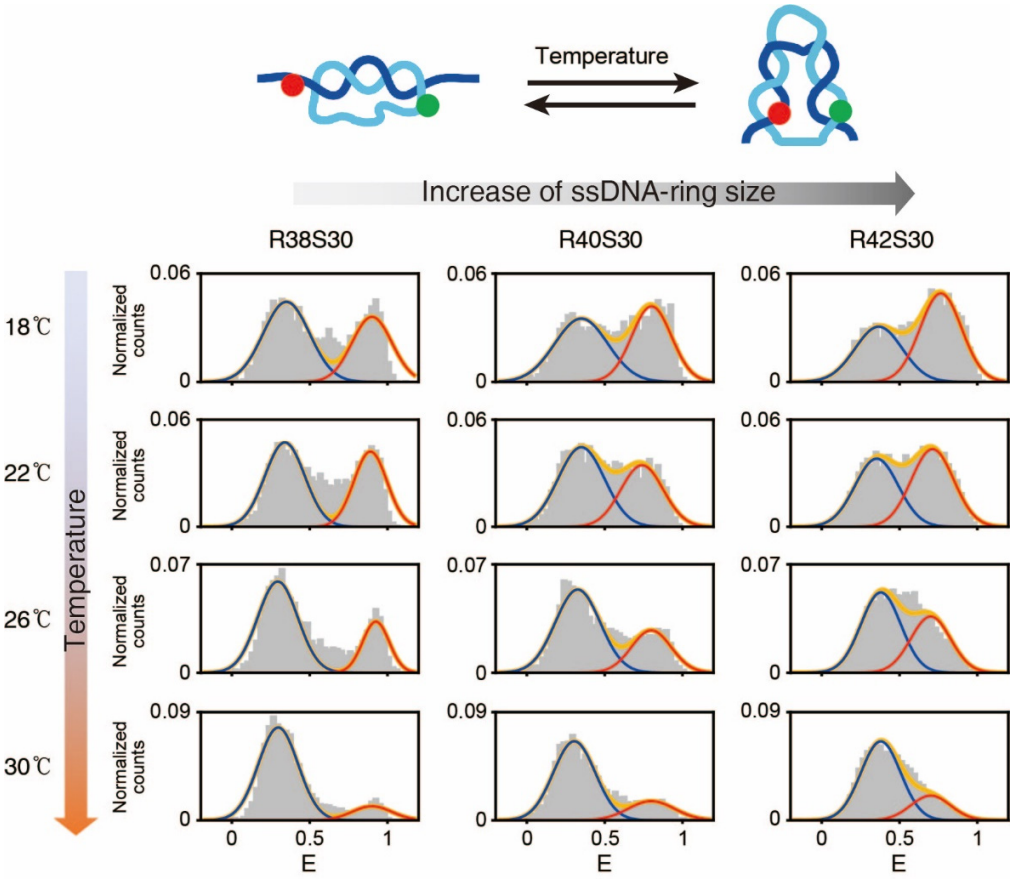

Supplementary Figure 5. FRET efficiency histograms for R38S30, R40S30, and R42S30 as a function of the temperature. The low FRET species sub-population (conformer I) increased as the temperature increased.

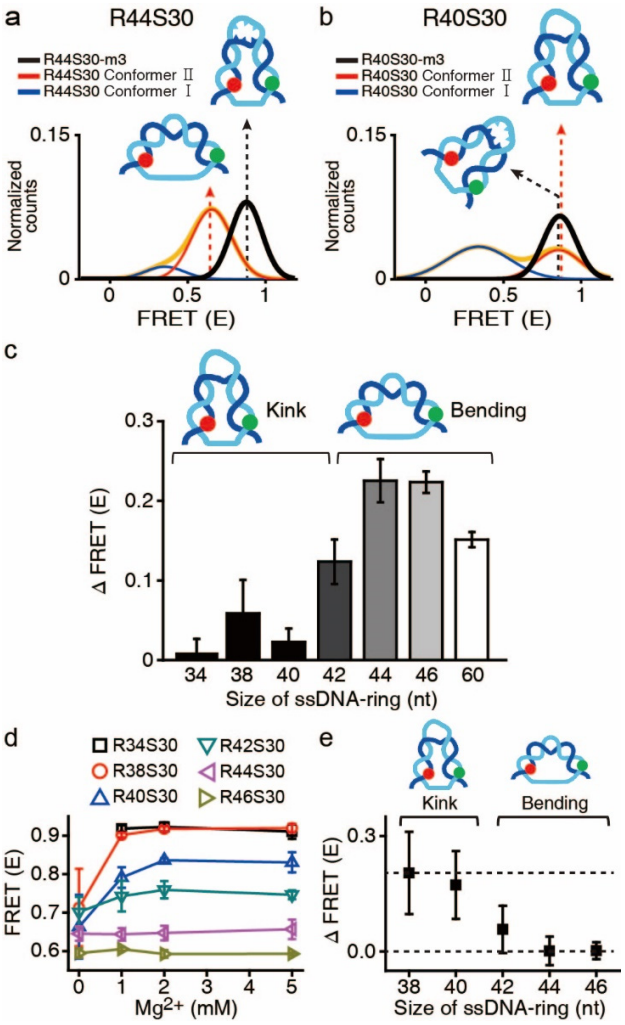

Supplementary Figure 6. Conformer II includes a kink with local melting. (a)-(b) A comparison of the FRET efficiency distributions between the intact and triple mismatched D-samples: (a) R44S30 and (b) R40S3. The black line denotes the FRET distribution for the triple mismatched D-samples, the red line indicates conformer II, and the blue line indicates conformer I of intact D-samples, respectively. (c) A bar graph showing the FRET efficiency differences between conformer II of the intact D-sample and the triple mismatched D-samples. (d) The FRET efficiency of conformer II as a function of the Mg^{2+} concentration. (e) The change in the FRET efficiency of conformer II between 0 mM and 2 mM Mg^{2+} from Supplementary Figure 6 d. All error bars were obtained from three independent measurements.

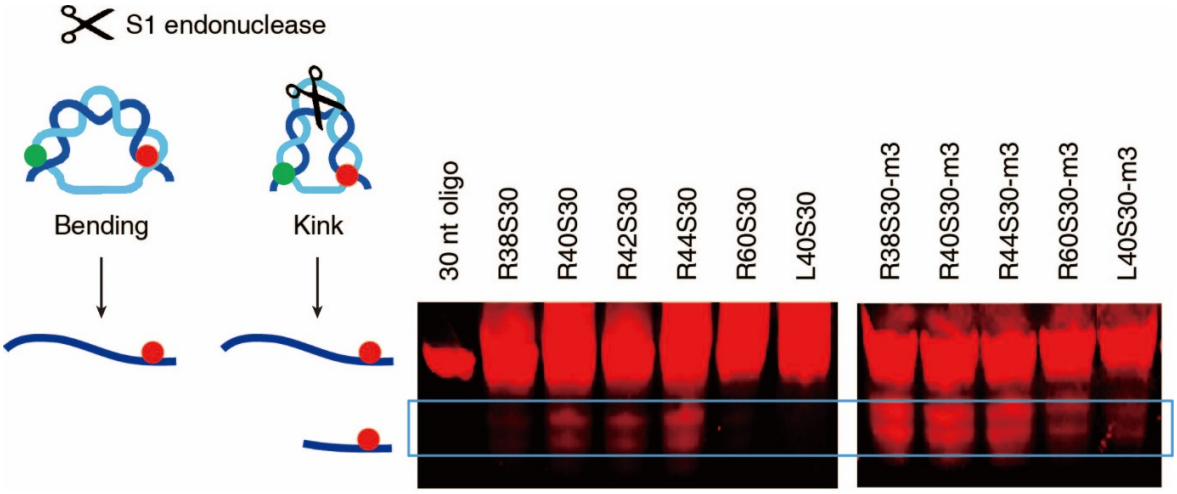

Supplementary Figure 7. S1 endonuclease cleavage test using the D-samples. If the D-samples include a bubble or local melting at the center of the dsDNA portion, S1 endonuclease cleaves the central region of the dsDNA portion, which yields short ssDNA fragments labeled with Atto-647N. *Left panel*: cartoon for S1 endonuclease activity and ssDNA products. *Right panel*: fluorescence images of the S1 endonuclease cleavage products. The Atto-647N fluorescent image was used to detect the S1 endonuclease cleavage products. We used "30 nt oligo" to denote a control for the 30 nt ssDNA without the S1 endonuclease treatment. The blue box denotes ssDNA products shorter than 30 nt ssDNA.

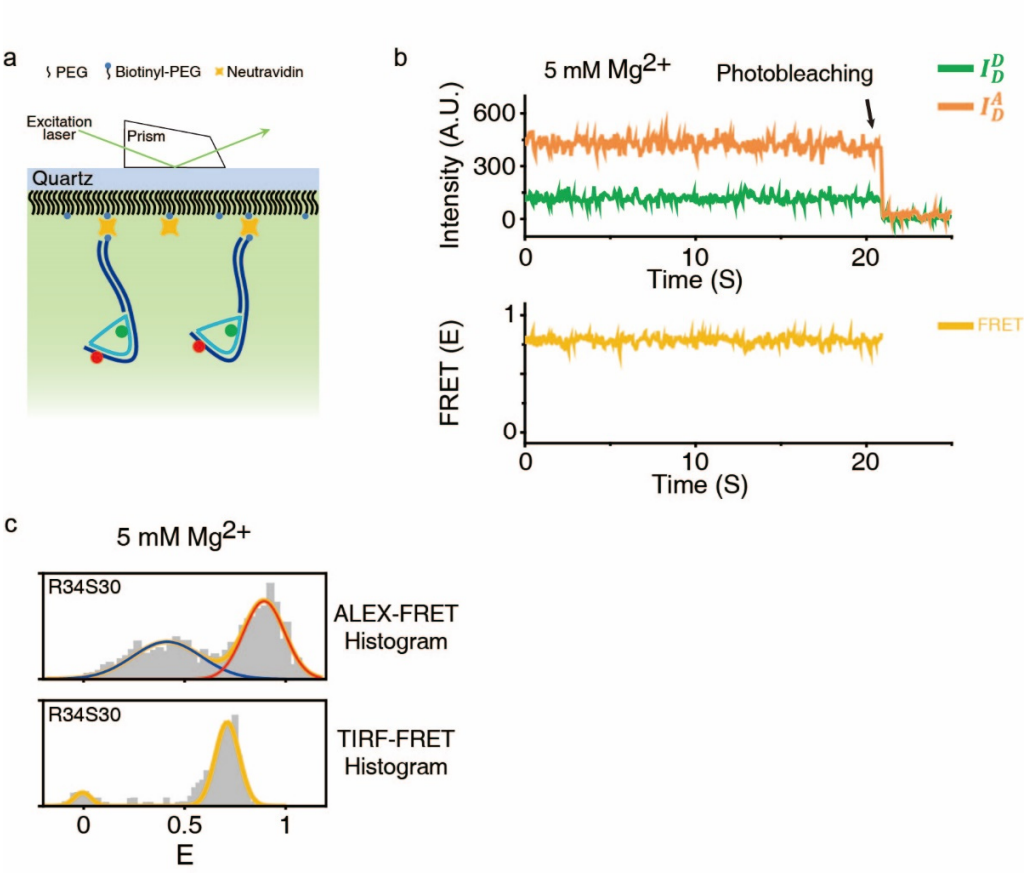

Supplementary Figure 8. Real-time measurement of FRET dynamics in the D-samples (R34S30) using total-internal reflection fluorescence microscopy (TIRF). (a) Schematic description of D-sample immobilization for TIRF measurements. Immobilized D-samples were prepared by annealing a 34 nt ssDNA ring with S30, which was extended using an 18 nt overhang (CCA/iAmMC6T/ATCAATAGGTGCGATCTGTTCTAAGGGCGACGGCTGAGCTCTAG). The 18 nt overhang was complementary to the ssDNA containing a biotin modification (/5Bio/CTAGAGCTCAGCCGTCGC), which was attached to the surface by biotin-Neutravidin interactions. In this sample, we labeled the 34 nt ssDNA ring and 18 nt extended S30 with Cy3 and Cy5, respectively. (b) Fluorescence intensity and FRET efficiency time traces using R34S30 immobilized on the surface. We did not observe a change in the FRET efficiency with a 100 ms temporal resolution. (c) Comparison the FRET efficiency histograms obtained using the ALEX method for freely diffusing molecules (upper panel) and the TIRF method for immobilized single molecules (bottom panel). The

temporal resolutions of FRET measurement were 1 ms and 100 ms for ALEX and TIRF, respectively.

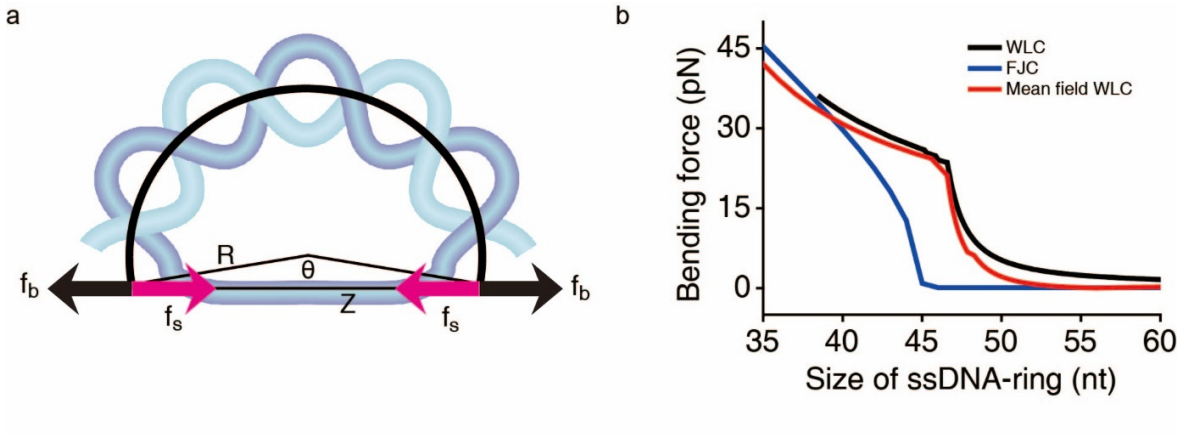

Supplementary Figure 9. (a) A sketch of the D-samples. The bending curvature of the dsDNA portion was calculated assuming that the bending force of the dsDNA portion is in equilibrium with the stretching force of the ssDNA portion. (b) The bending force as a function of the ssDNA ring size. The bending force of the dsDNA portion was calculated using the WLC model, while the ssDNA string stretching force was calculated using three types of models: the WLC model (black line), the freely joint chain (FJC) model (blue line), and the mean-field WLC model (red line).